

# General properties of the pion production reaction in nuclear matter

P. Camerini<sup>a,b</sup>, E. Fragiaco<sup>a,b</sup>, N. Grion<sup>a,1</sup>, S. Piano<sup>a,b</sup>, R. Rui<sup>a,b</sup>, J. Clark<sup>c</sup>, L. Felawka<sup>d</sup>,  
E.F. Gibson<sup>e</sup>, G. Hofman<sup>d</sup>, E.L. Mathie<sup>f</sup>, R. Meier<sup>g</sup>, G. Moloney<sup>c</sup>, D. Ottewell<sup>d</sup>, K.  
Raywood<sup>d</sup>, M.E. Sevier<sup>c</sup>, G.R. Smith<sup>d,2</sup>, and R. Tacik<sup>f</sup>.

<sup>a</sup> *Istituto Nazionale di Fisica Nucleare, 34127 Trieste, Italy*

<sup>b</sup> *Dipartimento di Fisica dell'Universita' di Trieste, 34127 Trieste, Italy*

<sup>c</sup> *School of Physics, University of Melbourne, Parkville, Vic., 3052, Australia*

<sup>d</sup> *TRIUMF, Vancouver, B.C., Canada V6T 2A3*

<sup>e</sup> *California State University, Sacramento CA 95819, USA*

<sup>f</sup> *University of Regina, Regina, Saskatchewan, Canada S4S 0A2*

<sup>g</sup> *Physikalisches Institut, Universität Tübingen, 72076 Tübingen, Germany.*

## The CHAOS Collaboration

The pion production reaction  $\pi^+ \rightarrow \pi^+\pi^\pm$  on  $^{45}\text{Sc}$  was studied at incident pion energies of  $T_{\pi^+} = 240, 260, 280, 300,$  and  $320$  MeV. The experiment was performed using the  $M11$  pion-channel at TRIUMF, and multiparticle events,  $(\pi^+, \pi^+\pi^\pm)$  and  $(\pi^+, \pi^+\pi^\pm p)$ , were detected with the CHAOS spectrometer. Results are reported in the form of both differential and total cross sections, and are compared to theoretical predictions and the reaction phase space. The present investigation of the T-dependence of the  $\pi^+A \rightarrow \pi^+\pi^\pm A'$  reaction complements earlier examinations of the A-dependence of the reaction, which was measured using  $^2\text{H}, ^4\text{He}, ^{12}\text{C}, ^{16}\text{O}, ^{40}\text{Ca},$  and  $^{208}\text{Pb}$  targets at  $\sim 280$  MeV. Some general properties of the pion-induced pion production reaction in nuclear matter will be presented, based on the combined results of the two studies.

PACS:25.80 Hp

---

<sup>1</sup>Corresponding author, electronic mail: Nevio.Grion@ts.INFN.it

<sup>2</sup>Permanent address: Jefferson Lab, Newport News, VA 23006

## 1. Introduction

The  $\pi^+ \rightarrow \pi^+\pi^\pm$  reactions ( $\pi 2\pi$ ) on  $^{45}\text{Sc}$  were studied at intermediate energies,  $T_{\pi^+} = 240, 260, 280, 300,$  and  $320$  MeV. The A-dependence of the  $\pi 2\pi$  process was studied previously on  $^2\text{H}, ^4\text{He}, ^{12}\text{C}, ^{16}\text{O}, ^{40}\text{Ca}$  and  $^{208}\text{Pb}$  nuclei at  $T_{\pi^+} \sim 280$  MeV [1, 2, 3, 4, 5, 6, 7]. The results of those investigations, combined with the present investigation of the  $\pi 2\pi$  T-dependence, allow for the determination of some general properties of the  $\pi 2\pi$  reaction in nuclei, as well as those of the  $\pi\pi$  system. The  $^2\text{H}$  studies were performed both to understand the  $\pi 2\pi$  behaviour on a neutron and a proton by means of the  $\pi N \rightarrow \pi\pi N$  quasifree reaction, and to observe medium modifications of the  $\pi\pi$  interaction through the direct comparison to the  $\pi 2\pi$  data in nuclei. To ensure a reliable comparison, all the  $\pi 2\pi$  data were taken under the same kinematical conditions.

The detection of  $\pi\pi$  pairs in the I=0 J=0 channel is a way of examining the existence of the light scalar-isoscalar meson, the  $\sigma$  meson. The direct observation of  $\sigma$ 's in vacuum has always been frustrated by the elusiveness of the meson, perhaps due to the large width of its spectral function [8]. The threshold behaviour of the  $(\pi\pi)_{I=J=0}$  system has been the subject of experimental investigations: the invariant mass intensities display a remarkable strength in nuclei, while they appear depleted in the nucleon (i.e., in vacuum) [7]. An interpretation of this observation relies on the partial restoration of chiral symmetry in nuclear matter. In a chiral symmetric space, chiral partners would have same spin but opposite parity, and be degenerate in mass. In this framework, the chiral partner of the  $\sigma$  ( $J^P = 0^+$ ) is the pion ( $J^P = 0^-$ ). These mesons, however, have the masses which are a few hundred MeV apart. The shift of the  $\pi\pi$  invariant mass toward the lower  $2m_\pi$  in nuclei is taken as a signature of partial restoration of the broken symmetry [9, 10]. It is worthwhile noting that this process is observed in nuclei, i.e. at nuclear densities  $\rho < \rho_n$  the saturation density. In the same environment, another process contributes to the reshaping of the  $(\pi\pi)_{I=J=0}$  spectral function at around the  $2m_\pi$  threshold (and below it), which is due to the P-wave coupling of pions to *particle-hole* ( $p$ - $h$ ) and *delta-hole* ( $\Delta$ - $h$ ) configurations. The net result is similar, although less pronounced, to that of partial restoration of chiral symmetry [11, 12, 13, 14, 15].

Correlated pion pairs have also been studied in a unitary chiral nonperturbative model [16]. In this approach, the  $\sigma$  resonance in vacuum is dynamically generated by the strong  $\pi\pi$  interaction. In nuclear matter, the  $\sigma$  properties are only weakly modified [17], whereas the  $(\pi\pi)_{I=J=0}$  interaction is altered by the P-wave coupling of pions to  $p$ - $h$  and  $\Delta$ - $h$  states. In the I=0 J=0 channel,  $ImT_{\pi\pi}$  enhances its strength at  $2m_\pi$  as pion pairs probe increasing  $\rho$ 's. The increase is detectable at  $\rho < \rho_n$ . The pion production reaction in nuclei proceeds via the quasifree  $\pi N \rightarrow \pi\pi N$  elementary process [18], and the nuclear influence on the process is accounted for by a complete model [15], which is considered the *state-of-the-art* in this field.

Table 1: Characteristics of the particle beam: Central momentum ( $p$ , [MeV/c]) and energy ( $T$ , [MeV]), momentum spread ( $\delta p/p$  at FWHM, [%]), intensity ( $N$ , [ $10^6$ particles/s]), and composition ( $\pi$ [%],  $p$ [%]).

$p$ , $T$	$\delta p/p$	$N$	$\pi$ , $p$
353, 240	2.0	1.6	95.5, 4.5
374, 260	1.1	3.4	94.3, 5.7
396, 280	1.1	2.6	94.9, 5.1
417, 300	1.0	2.4	95.7, 4.3
438, 320	1.6	1.5	96.4, 3.6

The purpose of the present article is to give an account of new results on the  $T$ -dependence of the  $\pi 2\pi$  reaction, and to examine the data in relation to the above mentioned theoretical results. In addition, complemented by the earlier studies of the  $A$ -dependence, general properties of the  $\pi 2\pi$  process in nuclear matter are sketched out. The  $\pi 2\pi$  data were collected under the same kinematical conditions to allow for a straightforward comparison of the results. Pion pairs were analysed down to opening angles  $\sim 0^\circ$  in order to determine the  $\pi\pi$  invariant mass at the  $2m_\pi$  threshold, and the energy of incident pions was limited to 320 MeV to reduce the final state interactions of pions with the residual nucleus. The article is organised as follows: some features of the experiment are reported in Sec. 2. Sec. 3 deals with the data analysis. Exclusive  $\pi 2\pi$  data at 300 MeV are discussed in Sec. 4. The  $\pi 2\pi$  model used for comparison is presented in Sec. 5. The  $T$ -dependence of the reaction is reported in Sec. 6. Other existing results are mentioned in Sec. 7. Finally, conclusions are summarised in Sec. 8.

## 2. The experiment at TRIUMF

The aim of the experiment was the measurement of differential cross sections for the  $\pi^+ \rightarrow \pi^+ \pi^\pm$  reactions at several incident pion kinetic energies. This required single particle mass-identification and vector momentum determination for each event.

### 2.1 The pion beam and the beam counting

The experiment was performed at the TRIUMF Meson Facility, using positive pions from the M11 channel. The final focus was located at the centre of the detector. Pion energies were 240, 260, 280, 300, and 320 MeV. Positive pions were accompanied by the  $\pi^+$ 's decay products, i.e.  $\mu^+$ 's and  $e^+e^-$ , and  $p$ 's. However, the contamination of positrons and positive muons was found to be less than 1% at all energies. Protons were initially separated from

pions by means of an absorber placed in the mid-plane of M11, and finally intercepted by the slits of the channel. Protons escaping the slits were constantly monitored through their time-of-flight along the beam line ( $\sim 13.5$  m long). The beam characteristics are summarised in Table 1. The target used was a solid slab of  $^{45}\text{Sc}$   $0.558$  g/cm $^2$  thick. The target area exposed to the pion beam was  $4.25 \times 3.03$  cm $^2$ , which could contain a large fraction of the beam envelope.

The number of pions impinging upon the target was constantly monitored by an in-beam scintillator counter, which was located at about 0.8 m from the target. Therefore, the real number of pions arriving at the target was corrected for the rate of pion decay, which was  $\sim 3.5\%$  at  $T_{\pi^+}=280$  MeV. In addition, a rate correction due to multiple pions per beam burst was applied; this was, for example,  $\sim 4.9\%$  at  $T_{\pi^+}=280$  MeV. Detailed calculations are reported in Ref. [7].

## 2.2 The CHAOS spectrometer

Multiparticle charged events were detected by the CHAOS spectrometer[19]. CHAOS consists of a dipole magnet, four cylindrical wire chambers (WC) and a cylindrical

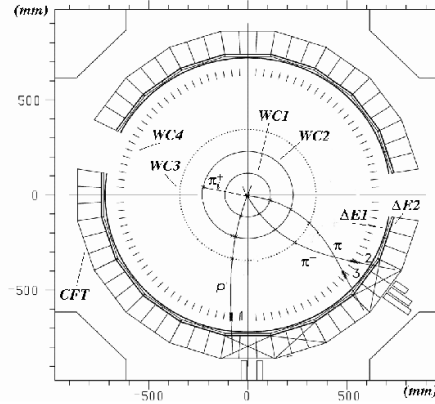


Figure 1: Reconstructed particle trajectories in CHAOS for  $\pi_i^+ \rightarrow \pi^+ \pi^- p$  at  $T_{\pi_i^+}=300$  MeV. The experimental layout shows the geometrical disposition of the wire chambers (WC), the first level trigger hardware (CFT) and the magnet return yokes in the corners. The CFT segments which are hit by particles are marked with crosses, and the energy deposited in the first two layers ( $\Delta E1$  and  $\Delta E2$ ) is indicated by boxes.  $\Delta E1$  is hit by two pions, however the thinner segmentation of  $\Delta E2$  is sufficient to distinguish them.

telescope of fast counters (CFT). Fig. 1 shows the geometrical disposition of the magnet return yokes, wire chambers and telescope, and the trajectories of a reconstructed event,  $\pi_i^+ \rightarrow \pi^+\pi^-p$  on  $^{45}\text{Sc}$  at  $T_{\pi^+}=300$  MeV. The magnetic field was varied with  $T_{\pi^+}$  to maintain constant the trajectory of the incident beam. The field was 0.55 T at  $T_{\pi^+}=240$  MeV and 0.69 at  $T_{\pi^+}=320$  MeV. The inner and the outer WC's have a diameter of  $\sim 23$  cm and  $\sim 123$  cm, respectively. The latter is a vector WC, which operates in the fringe field of the magnet. The overall WC efficiency to fully reconstructed  $\pi 2\pi$  events about  $50\pm 5\%$ . With this setup, the vector momentum  $\vec{p}_\pi(p, \Theta)$  of a 130 MeV/c pion was analysed with  $\delta p \sim 5$  MeV/c and  $\delta\Theta \leq 2^\circ$ . Both uncertainties are due mainly to pion multiple scattering. The CFT telescope encircles WC4. The CFT hardware is composed of two layers of NE110 plastic scintillator, 0.3 cm and 1.2 cm thick respectively, and a layer of SF5 lead-glass of  $\sim 5$  radiation lengths. The telescope is segmented. Each segment covers an azimuthal angle  $\Delta\Theta = 18^\circ$ . Segments can be removed to allow the pion beam to enter and exit CHAOS. The first CFT layer subtends the smallest zenith angle  $\Delta\Phi = \pm 7^\circ$ ; therefore, it defines the geometrical solid angle of CHAOS  $\Omega = 1.5$  sr. The necessity of removing 2 (out of 20) CFT segments during a measurement leads to a nonuniform acceptance of CHAOS. In addition, pions decaying inside CHAOS further increase the irregularity of the acceptance. Thus, GEANT Monte Carlo simulations were required, which resulted in assigning a weight to each  $\pi 2\pi$  event before it was binned. The weight distributions resemble those reported in Ref.[7] Fig. 4: they peak at  $weight \sim 1.5$  and monotonically decrease to zero at  $weight \sim 7$ . In order to avoid large corrections in the distributions, the soft cut  $0 < weight < \sigma + 2\mu$  on reconstructed events is applied, where  $\sigma$  and  $\mu$  are the mean value and the standard deviation of the weight distributions, respectively. In the case of  $T_{\pi^+}=300$  MeV,  $\sigma + 2\mu \sim 5.5$ .

### 2.3 Particle mass-identification

Incident pions produce background reactions whose rate overwhelms the  $\pi 2\pi$  rate. Therefore, to study the  $\pi 2\pi$  process in nuclei, a thorough identification of particle masses is required. In the case of CHAOS, this is accomplished by binding the momentum (polarity) of a particle to the pulse-height response of the telescope layers. In the present measurement, pion momenta do not exceed 230 MeV/c and the particles involved are  $\pi$ 's,  $e$ 's,  $p$ 's and  $d$ 's.

The pulse height response ( $PH$ ) of pions and protons in plastic scintillators is  $PH_p/PH_\pi > 5$  for  $p_\pi \leq 230$  MeV/c see Fig. 8 in Ref. [20] and Fig. 3 in Ref.[3]. By using only the first two CFT layers, pions were separated from protons (deuterons) with high ( $\sim 100\%$ ) selectivity. The same technique cannot favourably be applied to  $\pi$ 's and  $e$ 's for momenta exceeding 110 MeV/c. Thus, SF5 lead-glass Cherenkov counters were used.

Electrons (positrons) are byproducts of single charge exchange processes in the  $^{45}\text{Sc}$  target:  $\pi^+ \rightarrow \pi^0$  followed by  $\pi^0$  decay  $\pi^0 \rightarrow \gamma\gamma$  and  $\gamma$  conversion  $\gamma \rightarrow e^+e^-$ . Thus,  $e^+e^-$  pairs may look like  $\pi^+\pi^-$  pairs. Fig. 2 shows the opening angle distributions of  $e^+e^-$  ( $\Theta_{e^+e^-}$ ,

full squares) and  $\pi^+\pi^-$  ( $\Theta_{\pi^+\pi^-}$ , full diamonds) pairs for the 300 MeV run, where  $\Theta$  is defined in the lab frame as the difference of the azimuthal angles of reconstructed pairs. Most of the  $\Theta_{e^+e^-}$  strength occurs near  $0^\circ$ . An  $e^+e^-$  to  $\pi^+\pi^-$  misidentification would result in a contamination of  $\Theta_{\pi^+\pi^-}$  at around  $0^\circ$ , and thus in a contamination of the  $\pi^+\pi^-$  invariant mass at around the  $2m_\pi$  threshold (Ref. [7] Fig. 13). In order to safely separate electrons from pions, the following strategy was followed. Soft kinematical cuts were assigned to reject those  $\pi 2\pi$  spurious events whose momenta and total energy sum exceed the values allowed by the  $^{45}Sc(\pi^+, \pi^+\pi^-p)^{44}Sc$  phase space. The same soft cuts were also applied to  $e^+e^-$  pairs, which brings about the distributions in Fig. 2. The Cherenkov counters have a  $\pi$  to  $e$  discrimination efficiency above 95% for momenta below 230 MeV/c (Ref. [20] Fig. 11), which brings the  $e^+e^-$  to  $\pi^+\pi^-$  misidentification rate to about 0.25%. This is further reduced to about 0.1% by rejecting events with opening angles less than  $3^\circ$ . For the distributions shown in Fig. 2, there are about 3000  $\Theta_{e^+e^-}$  events between  $0^\circ$  and  $18^\circ$ , which is reduced to about 3 events by the CFT filtering combined with the  $3^\circ$  soft cut. These events would mainly affect the  $5^\circ$   $\Theta_{\pi^+\pi^-}$  datum which consists of about 900 events. Thus the surviving  $e^+e^-$  contaminants have a negligible impact on the opening angle distributions, and in general

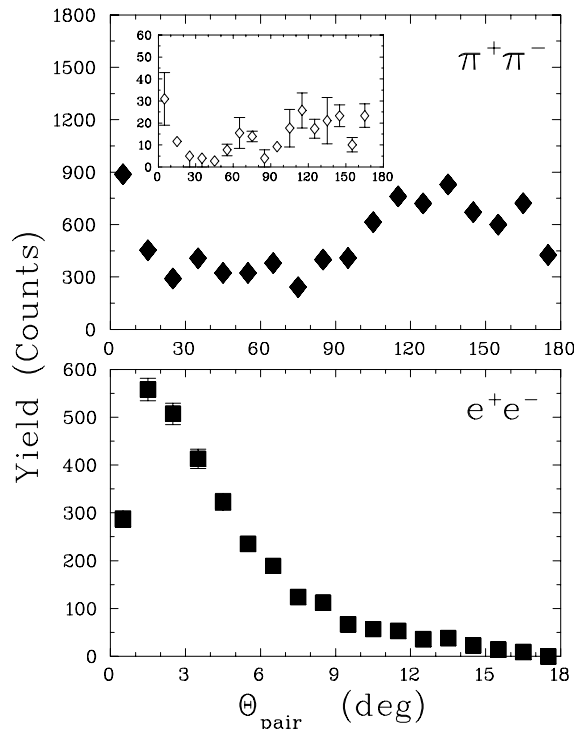


Figure 2: Opening angle distributions of  $e^+e^-$  (full squares) and  $\pi^+\pi^-$  (full diamonds) pairs at  $T_{\pi^+}=300$  MeV. The inset diagram shows the  $\pi^+\pi^-$  opening angle distribution (open diamonds) for the  $\pi^+ \rightarrow \pi^+\pi^-p$  reaction; in this case,  $\pi^+\pi^-$  pairs are detected in coincidence with protons.

on the  $\pi 2\pi$  spectra. This feature is common to all the examined energies. In the upper panel, of Fig. 2, the  $\Theta_{\pi^+\pi^-}$  distribution (open diamonds) is shown for pion pairs detected in coincidence with protons, namely, for pairs from the  $\pi^+ \rightarrow \pi^+\pi^-p$  reaction. In this case,

kinematical cuts on the kinetic energy sum of particles detected in the reaction exit channel ( $T_{SUM}$ ) avoid contributions from  $e^+e^-$  pairs in coincidence with a proton. Nevertheless, the two  $\Theta_{\pi^+\pi^-}$  distributions show a similar behaviour. This second self-reliant result confirms that  $e^+e^-$  events are efficiently rejected.

### 3. Analysis

The  $\pi 2\pi$  data are fully corrected within the geometrical acceptance of CHAOS. No attempt to correct for data outside the CHAOS acceptance has been made, since this would involve relying either on phase space simulations or on model calculations. Such a *model-dependent* approach would alter the shape of distributions; in fact, the data must be extrapolated over a large  $\Phi$ -interval without the assistance of experimental data. This is illustrated in Fig. 3 for the  $\pi\pi$  invariant mass distributions at  $T_\pi=280$  MeV: the full-line diagrams are the results of phase space simulations for the  $^{45}Sc(\pi^+, \pi^+\pi^\pm N)^{44}X$  reactions for an ideal  $4\pi$  detector, while the shaded diagrams depict the effects on distributions of the CHAOS geometry. In the present work, the shape of distributions will reflect the coplanar geometry of the spectrometer.

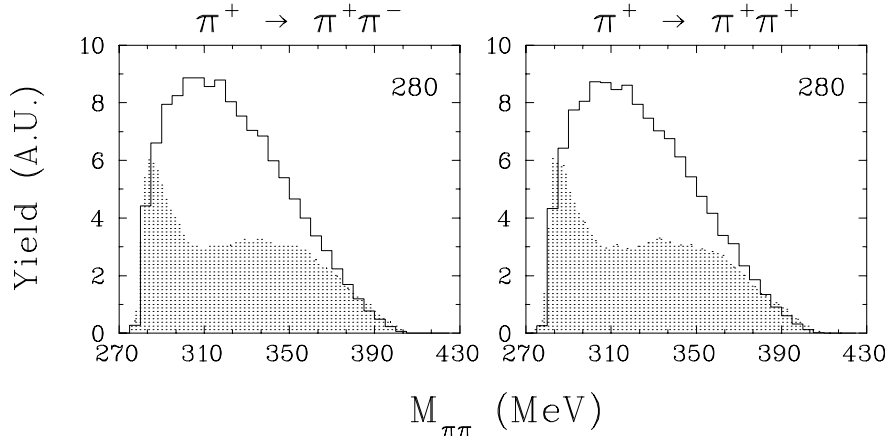


Figure 3: Results of phase space simulations for the  $^{45}Sc(\pi^+, \pi^+\pi^\pm N)^{44}X$  reactions at 280 MeV. Full-line diagrams:  $\pi\pi$  invariant mass distributions for an ideal  $4\pi$  detector; shaded diagrams:  $\pi\pi$  invariant mass distributions when including the CHAOS geometry. The diagrams are normalised at low and high invariant masses where distributions appear to have the same behaviour.

Once the particle mass is identified, the particle vector momenta are checked against simulations of the  $^{45}Sc(\pi^+, \pi^+\pi^\pm N)^{44}X$  phase space, which include the CHAOS acceptance and resolution. A reconstructed event is rejected when it exceeds the allowed phase space volume. This procedure is applied to all the five energies. As an example, for the 300 MeV run the following soft cuts are applied:  $p_{\pi^+} < 215$  MeV/c,  $p_{\pi^-} < 215$  MeV/c and  $T_{SUM} < 156$  MeV. As earlier mentioned, each  $\pi 2\pi$  event is weighted before being binned. In order to

avoid large corrections, the soft cut  $0 < weight < 5.5$  on reconstructed events is applied. In the case of the  $\pi^+ \rightarrow \pi^+\pi^-$  channel, the number of reconstructed events which passed the above tests are several thousands for each energy. The number drops by an order of magnitude for the  $\pi^+ \rightarrow \pi^+\pi^+$  channel.

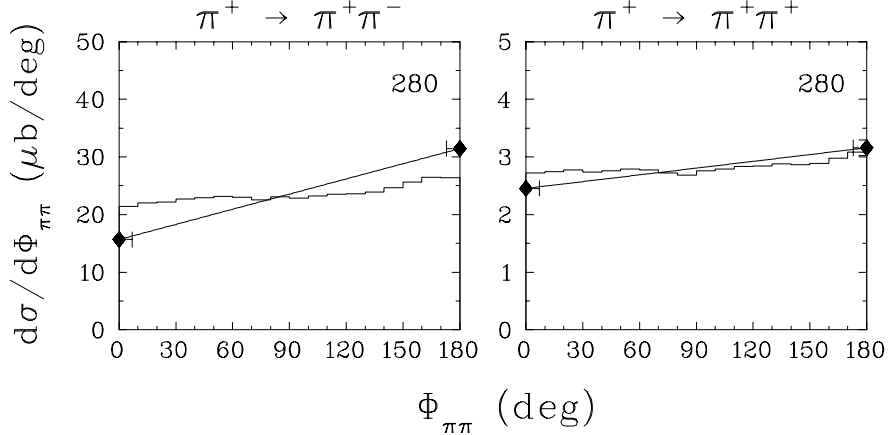


Figure 4: Out-of-plane dependence of  $d\sigma/d\Phi_{\pi\pi}$  as a function of  $\Phi_{\pi\pi} \equiv \Phi_{\pi_1\pi_2} = |\Phi_{\pi_1} - \Phi_{\pi_2}|$  for the  $\pi^+ \rightarrow \pi^+\pi^\pm$  reaction channels at  $T_{\pi^+}=280$  MeV. Full diamonds: experimental points; full lines: curves linearly joining the experimental data; full histograms: results of phase-space simulations for the  $^{45}Sc(\pi^+, \pi^+\pi^\pm N)^{44}X$  reactions normalised to the data at  $0^\circ \pm 7^\circ$  and  $180^\circ \pm 7^\circ$ .

The data reduction is based on  $\pi \rightarrow \pi_1\pi_2$  events which passed the following tests: have the origin in the target region, be mass- and charge-identified, survive the tests on kinematics and weights. Many-fold differential cross sections  $d^4\sigma/(dTd\Omega)_{\pi_1}(dTd\Omega)_{\pi_2}$  are then formed, where  $T$  is the kinetic energy of a final pion and  $\Omega$  is the solid angle into which a pion is scattered.  $\Omega_\pi$  is related to the zenithal angle  $\Phi_\pi$  and the azimuthal angle  $\Theta_\pi$  via the equation  $d\Omega_\pi = d\cos(\Theta_\pi)d\Phi_\pi$ . The two angles reflect the coplanar geometry of CHAOS, which restricts the out-of-plane acceptance to vary within  $\pm 7^\circ$ , while particles are accepted from  $0^\circ$  to  $360^\circ$  in the plane of the reaction except for two angular segments each  $18^\circ$  wide. The latter account for the removal of two CFT's which allow the pion beam to enter and exit CHAOS (see Fig. 1). The data are represented as triple differential cross sections  $d^3\sigma/d\mathcal{O}_{\pi\pi}d\Omega_\pi d\Omega_\pi$ , where  $\mathcal{O}_{\pi\pi}$  represents  $(T$  or  $\Theta)_{\pi\pi}$  or a combination of them, and  $\pi$  denotes a charged pion.  $\frac{d^3\sigma}{d\mathcal{O}d\Omega d\Omega}$  is determined by the quantities  $f_e \frac{N(\mathcal{O})}{\Delta\mathcal{O}}$ , where  $f_e$  is a parameter which is determined by the experimental conditions,  $N(\mathcal{O})$  is the number of weighted events in a given bin and  $\Delta\mathcal{O}$  is the bin width for the  $\mathcal{O}$  observable. The systematic uncertainty in assessing  $f_e$  is 13.4% ( $\sigma$ ) at the central energy  $T_{\pi^+}=280$  meV. A more detailed analysis for  $T_{\pi^+}=280$  MeV is reported in Ref.[7]. The error bars reported on the  $\pi 2\pi$  spectra account only for the statistical uncertainty. The overall uncertainty is obtained by summing the systematic and the statistical uncertainties in quadrature. In order to obtain the total cross section  $\sigma_T$ , the differential cross section  $d^3\sigma/d\mathcal{O}_{\pi\pi}d\Omega_\pi d\Omega_\pi$  is summed over  $\mathcal{O}_{\pi\pi}$  and  $\Omega_\pi$ 's. Fig. 4 illustrates the out-of-plane dependence of the cross section  $d\sigma/d\Phi_{\pi\pi}$  at 280 MeV, where  $\Phi_{\pi\pi} \equiv \Phi_{\pi_1\pi_2} = |\Phi_{\pi_1} - \Phi_{\pi_2}|$ . The integration over the unmeasured portion of  $\Phi_{\pi\pi}$



is accomplished either by using a linear function joining  $\Phi_{\pi\pi} = 0^\circ$  to  $\Phi_{\pi\pi} = 180^\circ$ , or by interpolating the two measured points with the reaction phase space. Such an approach is applied to all the incident pion energies and the results are similar. The values of  $\sigma_T$  so obtained are listed in table 2 (Sec. 6.4).

#### 4. The $\pi^+ \rightarrow \pi^+\pi^-p$ exclusive measurement at $T_{\pi^+}=260$ and 300 MeV.

At  $T_{\pi^+}=300$  MeV kinetic energy, the  $\pi^+\pi^-$  data were collected with sufficient statistics (over  $10^4$  reconstructed events) to enable an analysis of the  $\pi^+(n) \rightarrow \pi^+\pi^-p$  exclusive reaction channel. Some results are discussed below.

Fig. 5 shows the missing energy ( $E_M$ ) distribution of the  $\pi^+ {}^{45}\text{Sc} \rightarrow \pi^+\pi^-p {}^{44}\text{Sc}$  reaction at  $T_{\pi^+}=260$  and 300 MeV. The missing energy is defined by the equation  $E_M = [M_{{}^{45}\text{Sc}} - M_{{}^{44}\text{Sc}} - m_\pi - m_p] - [T_{\pi^+}^f + T_{\pi^-}^f + T_p^f - T_{\pi^+}^i]$ , where the symbol  $M(m)$  indicates a nucleus

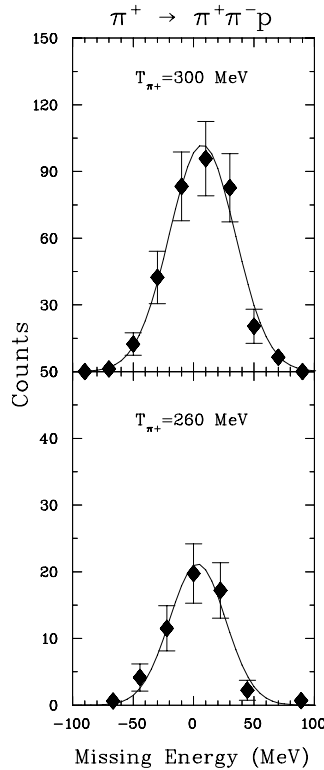


Figure 5: Missing energy distributions of the  $\pi^+ {}^{45}\text{Sc} \rightarrow \pi^+\pi^-p {}^{44}\text{Sc}$  reaction at incident kinetic energies of 260 and 300 MeV. The definition of missing energy is given in the text; in this case,  $\pi^+\pi^-$  pairs are detected in coincidence with protons. The curves are a Gaussian fit to the data.

(particle) mass, while  $i$  and  $f$  denote the initial and final particles, respectively. In this framework,  $E_M$  represents the excitation energy of the  ${}^{44}\text{Sc}$  residual system. The  $E_M$  mean values, obtained with a Gaussian fit to the data, are  $\sim 7$  MeV at  $T_{\pi^+}=300$  MeV, and  $\sim 3$

MeV at  $T_{\pi^+}=260$  MeV. These values are consistent with  $E_M \sim 0$  MeV, when considering that the residual nucleus may be left in an excited state. Therefore, the  $\pi \rightarrow \pi\pi$  reaction at intermediate energies is a quasifree process, which mainly involves a single nucleon  $\pi N \rightarrow \pi\pi N$ . A similar result was found in Ref.[3], where the  $\pi 2\pi$  reaction was studied as a function of the nuclear mass number.

Fig. 6 shows the invariant mass distributions (shaded diagrams) of  $\pi^+\pi^\pm$  pairs that are detected without the requirement of a proton in coincidence. The  $M_{\pi\pi}$  distributions are also plotted as a function of  $p_{\pi\pi} = |\vec{p}_{\pi^+} + \vec{p}_{\pi^\pm}|$ , in order to illustrate the  $p_{\pi\pi}$ -dependence of  $M_{\pi\pi}$  for the two reaction channels. The two channels have a similar behaviour: the low  $M_{\pi\pi}$  bins

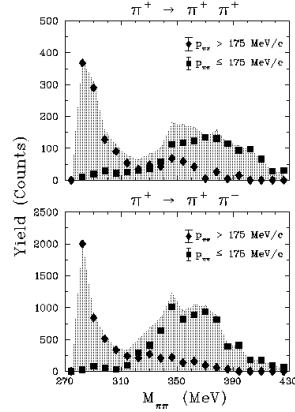


Figure 6: Invariant mass distributions of  $\pi^+\pi^\pm$  pairs at 300 MeV for  $^{45}\text{Sc}$  as a function of  $p_{\pi\pi}$ , the magnitude of the pion pair momentum. Shaded diagrams  $0 \leq p_{\pi\pi} \leq 350$  MeV/c (the maximum momentum reached by a pion pair), full squares  $0 \leq p_{\pi\pi} \leq 175$  MeV/c, and full diamonds  $175 < p_{\pi\pi} \leq 350$  MeV/c.

are mainly populated by pairs (full diamonds) with the highest momenta  $p_{\pi\pi} > 175$  MeV/c. These pairs, however, show a different behaviour when their opening angle distributions are compared. Fig. 7 depicts the  $\Theta_{\pi\pi}$  distributions for  $p_{\pi\pi} > 175$  MeV/c and  $2m_\pi \leq M_{\pi\pi} \leq 310$  MeV. In this invariant mass range,  $\pi^+\pi^+$  (open diamonds) and  $\pi^+\pi^-$  (full diamonds) pairs are known to carry  $I=2$   $J=0$  and  $I=0$   $J=0$  quantum numbers, respectively [1, 7, 15, 21]. The  $\Theta_{\pi^+\pi^+}$  distribution is well described by the  $\pi^+ {}^{45}\text{Sc} \rightarrow \pi^+\pi^+n {}^{44}\text{Ca}$  phase space (full line). On the other hand, the  $\Theta_{\pi^+\pi^-}$  distribution displays a sharp peak at around  $0^\circ$ , before continuing as  $\pi^+ {}^{45}\text{Sc} \rightarrow \pi^+\pi^-p {}^{44}\text{Sc}$  phase space (double line). For both channels, simulations include the CHAOS acceptance as well as the  $p_{\pi\pi}$  and  $M_{\pi\pi}$  cuts, and are normalised to the data from  $\Theta_{\pi\pi} > 25^\circ$ . In the case examined, the only difference between  $\pi^+\pi^+$  and  $\pi^+\pi^-$  pair is their quantum numbers, demonstrating the strong influence of nuclear matter on the  $(\pi\pi)_{I=J=0}$  interaction. Low  $M_{\pi^+\pi^-}$  are populated by  $(\pi\pi)_{I=J=0}$  pairs which decay preferentially with small  $\Theta_{\pi\pi}$  and high  $p_{\pi\pi}$ .

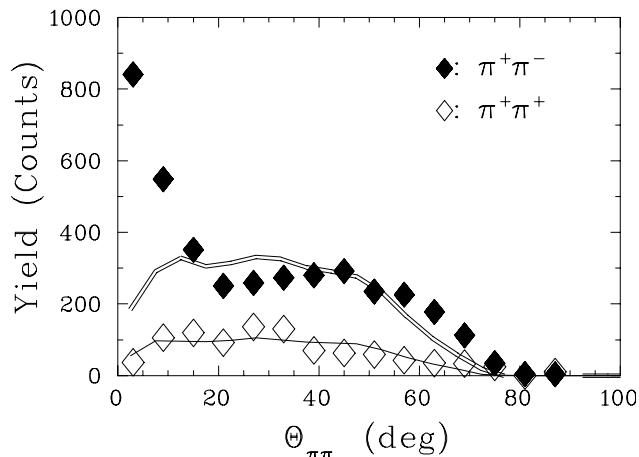


Figure 7: Opening angle distributions of  $\pi^+\pi^+$  and  $\pi^+\pi^-$  pairs at 300 MeV, for  $175 < p_{\pi\pi} \leq 350$  MeV/c and  $2m_\pi \leq M_{\pi\pi} \leq 310$ . The full and double lines are the results of phase space simulations for the reactions  $\pi^+ {}^{45}\text{Sc} \rightarrow \pi^+\pi^+n {}^{44}\text{Ca}$  and  $\pi^+ {}^{45}\text{Sc} \rightarrow \pi^+\pi^-p {}^{44}\text{Sc}$ , respectively. Simulations include the CHAOS acceptance as well as the  $p_{\pi\pi}$  and  $M_{\pi\pi}$  cuts, and are normalised to the data from  $\Theta_{\pi\pi} > 25^\circ$ .

## 5. Model of the $\pi 2\pi$ reaction in nuclear matter

The experimental results will be compared with the model predictions of Ref. [15]. There are several good reasons for doing so. The calculation of the  $\pi 2\pi$  cross sections is based on a Monte Carlo method, which permits the CHAOS acceptance to be easily implemented in the code. The code requires the energy of the incident pion as an input parameter, thus the experimental distributions can be compared with the cross sections precisely at the same energies. For each accepted event, the code returns the vector momentum of each pion. A similar approach is followed in the data analysis, facilitating the comparison between calculated cross sections and distributions of experimental observables.

The model describes the elementary pion production reaction by involving only one nucleon of the nucleus, via the quasifree process  $\pi N \rightarrow \pi\pi N$  [15, 18]. The construction of the  $\pi N \rightarrow \pi\pi N$  amplitude relies on one-point diagrams, which include both the pion-pole and contact term, and two- and three-point diagrams. Nucleons as well as the  $\Delta(1232)$  and  $N^*(1440)$  can be excited as intermediate states. Standard nuclear effects, which may modify the reaction cross section, are accounted for. These include Fermi motion, Pauli blocking, pion absorption and quasielastic scattering. The role played by the nuclear medium on  $(\pi\pi)_{I=J=0}$  interacting pairs is carefully examined. A tangible modification of the  $\pi\pi$  interaction is determined by the coupling of pions to  $p$ - $h$  and  $\Delta$ - $h$  states, which enhances the intensity of the  $\pi\pi$  spectral function at around the  $2m_\pi$  threshold. The effects of the nuclear medium on the  $\sigma$  meson properties are analysed in separate articles [16, 17]. The  $\sigma$  mesons are dynamically generated by the rescattering of  $(\pi\pi)_{I=J=0}$  pions. Medium modifications are studied by coupling  $\sigma$ 's to the nucleons by means of tadpole diagrams. Once inserted

into the model, the tadpole terms are found to contribute negligibly. Therefore, the only detectable nuclear medium modification on the  $(\pi\pi)_{I=J=0}$  system comes from the P-wave coupling of pions to  $p$ - $h$  and  $\Delta$ - $h$  configurations. The model is able to predict the probability

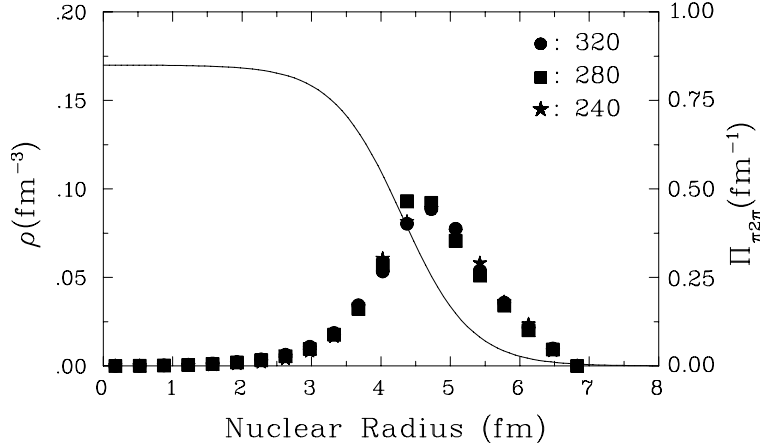


Figure 8: Nuclear density distribution ( $\rho$ , full curve) as a function on the nuclear radius for  $^{45}\text{Sc}$ . The probability of a  $\pi 2\pi$  event to occur ( $\Pi_{\pi 2\pi}$ ) is described by the distributions of the solid points: circles 320 MeV (energy of incident pions), squares 280 MeV and stars 240 MeV. The  $\Pi_{\pi 2\pi}$  distributions are normalized to unity, the  $\Pi_{\pi 2\pi}$  and  $\rho$  yields are calculated with the model of Ref. [15].

distribution of an interesting observable  $\Pi_{\pi 2\pi}$ , which cannot be measured.  $\Pi_{\pi 2\pi}$  is the composite probability of a  $\pi 2\pi$  event to take place and be detected (by CHAOS) as a function of the nuclear radius. Fig. 8 shows the distributions for various energies of incident pions: circles 320 MeV, squares 280 MeV and stars 240 MeV. The  $\Pi_{\pi 2\pi}$  distributions, when normalized to unity, vary slightly with energy thus indicating minor variations of the (average) nuclear density at which a  $\pi 2\pi$  event occurs. In fact,  $\rho=0.36\rho_n$  at  $T_{\pi^+}=320$  MeV,  $\rho=0.37\rho_n$  at  $T_{\pi^+}=280$  MeV, and  $\rho=0.35\rho_n$  at  $T_{\pi^+}=240$  MeV.

## 6. The T-dependence of the $\pi^+ \rightarrow \pi^+\pi^\pm$ reactions in $^{45}\text{Sc}$

The experimental results are compared with the predictions of the model described in Sec. 5, and with the phase space of the  $\pi^+ ^{45}\text{Sc} \rightarrow \pi^+\pi^\pm N ^{44}\text{X}$  reactions. Both model and phase space take the  $\pi 2\pi$  CHAOS acceptance into account. The error bars reflect statistical uncertainties. Systematic uncertainties for  $T_{\pi^+}=280$  MeV were discussed in Sec. 3.

### 6.1 The $\pi\pi$ invariant mass, $M_{\pi\pi}$

In order to check the consistency of the results, the  $M_{\pi\pi}^{\text{Sc}}$  distribution at 280 MeV is compared to the published  $M_{\pi\pi}^{\text{Ca}}$  cross section at 283 MeV [7]. The comparison is shown in Fig. 9 top panels for the  $\pi^+ \rightarrow \pi^+\pi^\pm$  reaction channels. The invariant mass of Sc (full diamonds) is normalised to the Ca invariant mass (open diamonds): as expected, the two distributions

display similar shapes since both kinetic energy and nucleus mass number are close. The

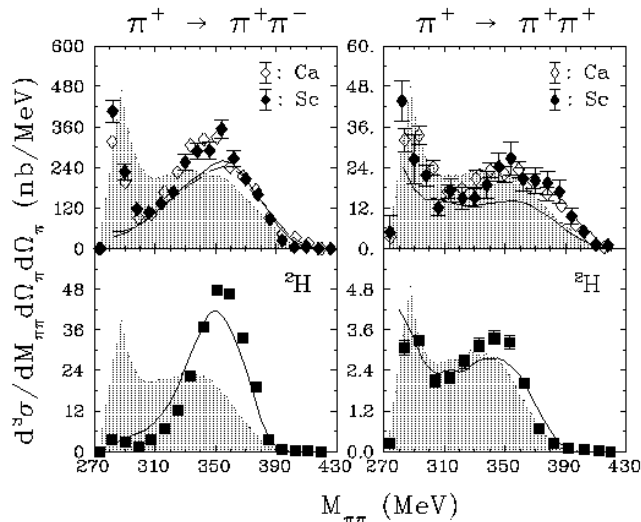


Figure 9: Invariant mass distributions of pion pairs for the  $\pi^+ \rightarrow \pi^+\pi^\pm$  reaction channels. The Ca data (open diamonds, [7]) were taken at 283 MeV and are used for normalisation. The Sc  $M_{\pi\pi}$  data are indicated with full diamonds and were taken at 280 MeV. The phase space of the  $^{45}\text{Sc}(\pi^+, \pi^+\pi^\pm N)^{44}\text{X}$  reactions are represented by the shaded diagrams. The curves are from [15, 16, 17]. The continuous lines denote the results of the full model. The dashed line in the upper left panel is obtained when pions are coupled only to  $p$ - $h$  and  $\Delta$ - $h$  states. More details are given in the text.

data (full squares) in the lower panels are the  $\pi\pi$  invariant mass distributions in deuterium, namely, of the elementary reactions  $\pi^+n(p) \rightarrow \pi^+\pi^-p(p)$  and  $\pi^+p(n) \rightarrow \pi^+\pi^+n(n)$  [7]. The data are compared with the model predictions (full line) described in Sec. 5 Ref. [15]. The noticeable feature is that, for the reactions on  $^2\text{H}$ , the calculations are able to reproduce the varying behaviour of the  $M_{\pi\pi}$  distributions at around threshold:  $M_{\pi^+\pi^-}$  is weakened to nearly zero while  $M_{\pi^+\pi^+}$  reaches its maximum.

In nuclei (Ca or Sc, upper panels) the situation changes. The  $M_{\pi^+\pi^+}$  distributions resemble that of the elementary reaction and are well explained by the model predictions (solid

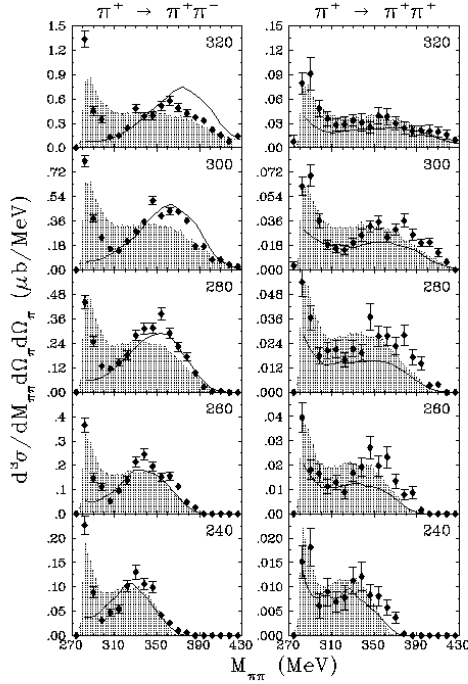


Figure 10: Invariant mass distributions of pion pairs as a function of the incident pion kinetic energy. The phase space for  ${}^{45}\text{Sc}(\pi^+, \pi^+\pi^\pm N){}^{44}\text{X}$  reactions is indicated by the shaded diagrams. The full lines are the model calculations of [15, 16, 17]. The kinetic energy of the pion beam is given in each panel.

line). In the  $\pi^+ \rightarrow \pi^+\pi^-$  channel,  $M_{\pi\pi}$  displays a remarkable reshaping with respect to the elementary process, and the fully renormalised calculations (solid line) give only a partial account of the threshold enhancement of the data. Furthermore, the invariant mass intensity decreases slightly at around threshold when only the P-wave coupling of pions to  $p$ - $h$  and  $\Delta$ - $h$  states is considered (dashed line).

A further element of comparison is the reaction phase space (shaded diagrams in Fig. 9), which is normalised to data. Phase space describes the  $M_{\pi^+\pi^+}$  distributions throughout the energy range, but largely misses the  $M_{\pi^+\pi^-}$  distributions.

The features observed for Sc at 280 MeV are in general observed at all the examined energies. This is illustrated in Fig. 10, which shows the  $M_{\pi^+\pi^\pm}$  cross sections as a function of the incident pion kinetic energy. The  $\pi^+\pi^+$  invariant mass cross section is well explained by a microscopic model of the pion production reaction [15], and the distributions are also described by the  $\pi 2\pi$  phase space. This leads to the following conclusions. The dynamical traits of the  $(\pi\pi)_{I=2J=0}$  interaction are understood, whether it occurs on the nucleon or in

nuclei. Furthermore, the nuclear medium does not appreciably change the  $\pi\pi$  interaction in the  $I=2$   $J=0$  channel with respect to the vacuum.

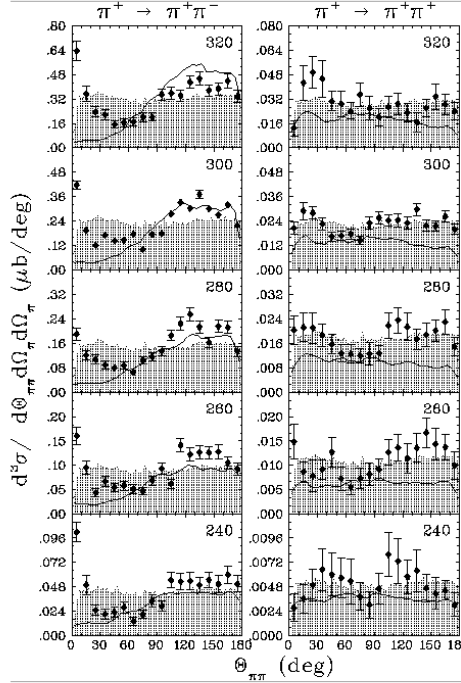


Figure 11: Opening angle distributions of pion pairs as function of the incident pion kinetic energy (full diamonds). The phase space of the  $^{45}\text{Sc}(\pi^+, \pi^+ \pi^\pm N)^{44}\text{X}$  reactions is indicated by the shaded diagrams. The full lines are the model calculations of [15, 16, 17]. The pion incident energy is given in each panel.

In the  $\pi^+ \rightarrow \pi^+ \pi^-$  channel, the terms describing the  $\pi N \rightarrow \pi\pi N$  amplitude must largely cancel out to explain the threshold depletion present in the model calculations. This view is also corroborated by the phase space behaviour, which approaches its maximum at around threshold. The enhancement measured at different kinetic energies (and nuclei) is only partly explained by theory, thus implying that either the cancellations are no longer effective in nuclear matter, or the  $\sigma$  (i.e., strongly interacting  $(\pi\pi)_{I=J=0}$  pairs) and its coupling to nucleons is not properly accounted for. In fact, other models of the  $(\pi\pi)_{I=J=0}$  interaction in nuclear matter [9, 10] find that the appearance of the  $\sigma$  largely contributes to heighten the  $\pi\pi$  spectral function at threshold. These models, however, do not embed any pion production process. As a final comment, it is worthwhile noting that all the  $\pi^2\pi$  data are well reproduced by both theory and phase space over the high invariant mass range.

## 6.2 The $\pi\pi$ opening angle, $\Theta_{\pi\pi}$

For a reconstructed pion pair  $\pi_1\pi_2$ , the opening angle is defined as  $\Theta_{\pi_1\pi_2} = \Theta_{\pi_1} - \Theta_{\pi_2}$ , where the azimuthal angles  $\Theta_{\pi_1}$  and  $\Theta_{\pi_2}$  are measured in the lab system. The indices 1 and 2 are assigned such that  $\Theta_{\pi_1\pi_2}$  is restricted to vary from  $0^\circ$  to  $180^\circ$ . The  $\pi\pi$  opening angle is an observable that proved to be sensitive to the isospin state of pion pairs (see Sec. 4 Fig. 7). The  $\Theta_{\pi\pi}$  distributions are presented in Fig. 11 for all the examined energies, and compared with the reaction theory and phase space. In the  $\pi^+ \rightarrow \pi^+\pi^+$  channel, the  $\Theta_{\pi\pi}$  distributions are generally flat over the angular interval  $0^\circ$ - $180^\circ$ . Such behaviour is predicted by the theory and phase space. The  $\Theta_{\pi^+\pi^-}$  distributions are peaked at around  $\sim 0^\circ$ , regardless of the energy. Such a feature is not described by the model calculations, which predict a smooth and decreasing intensity of  $\Theta_{\pi\pi}$  when approaching zero degrees. For the sake of comparison, in Fig. 12, the  $\Theta_{\pi\pi}$  distributions for the elementary reactions  $\pi^+n(p) \rightarrow \pi^+\pi^-p(p)$  and  $\pi^+p(n) \rightarrow \pi^+\pi^+n(n)$  at  $T_{\pi^+}=283$  MeV [5, 7] are shown.  $\Theta_{\pi^+\pi^-}$  is characterised by a negligible strength below  $\sim 60^\circ$ . In this angular span, the strength

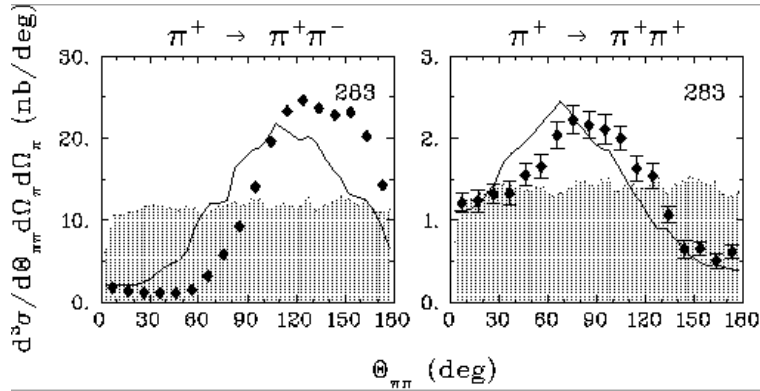


Figure 12: Opening angle distributions at 283 MeV kinetic energy. The shaded diagrams denote the phase space of the  ${}^2H(\pi^+, \pi^+\pi^\pm N)N$  reactions. The full lines are the model calculations of Refs. [15, 16, 17].

detected in nuclei is a direct consequence of the medium modifications on the  $(\pi\pi)_{I=J=0}$  interaction, since the  $\pi N \rightarrow \pi\pi N$  reaction is a quasifree process. The  $\pi^+ \rightarrow \pi^+\pi^+$  channel behaves differently. The elementary reaction already exhibits strength below  $60^\circ$ , which does not increase in Sc. Theory [15] is able to predict both the intensity and the shape of the  $\Theta_{\pi^+\pi^+}$  distributions for Sc. For  ${}^2H$ , calculations account correctly for the measured intensities over the interval  $0^\circ \leq \Theta_{\pi^+\pi^+} < 180^\circ$ , but the distribution is predicted to peak at about  $60^\circ$ ,  $20^\circ$ - $25^\circ$  below the measured value.

For the  $\pi\pi$  opening angle analysis, the conclusions that can be drawn are similar to those for the invariant mass. At intermediate energies, nuclear matter clearly modifies the  $(\pi\pi)_{I=J=0}$  interaction, while it leaves the  $(\pi\pi)_{I=2J=0}$  interaction rather unaltered. The theory is able to explain the  $\pi 2\pi$  process only when it occurs in the  $I=2$   $J=0$  channel.

### 6.3 The $\pi$ kinetic energy, $T_\pi$ .



The observable under consideration, and illustrated in Fig. 13, is the kinetic energy of a single pion. In the  $\pi^+ \rightarrow \pi^+\pi^-$  channel, positive (full diamonds) and negative (open

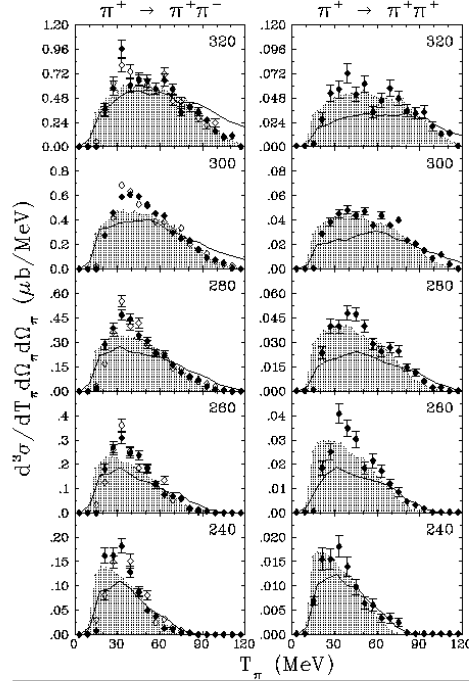


Figure 13: Single pion kinetic energy distributions as a function of the incident pion kinetic energy. Positive pion distributions are indicated with full diamonds, negative pions with open diamonds. The shaded diagrams are the result of phase space simulations for the  $\pi^+ {}^{45}\text{Sc} \rightarrow \pi^+\pi^\pm N {}^{44}\text{X}$  reactions. The full lines are the positive pion energy distributions which are derived from the model of Refs. [15, 16, 17].

diamonds) pion distributions can barely be distinguished throughout the energy range examined. The full lines [15] describe the positive pion energy distributions. Calculations provide a fair description of the measured distributions, but tend to overestimate the intensities of the data in the high-energy range. They predict greater abundances of energetic pions, which are also in excess of those expected from  $\pi^+ {}^{45}\text{Sc} \rightarrow \pi^+\pi^- p {}^{44}\text{Sc}$  phase space (shaded diagram). The  $T_{\pi^+}$  distributions are well accounted for by the  $\pi^+ {}^{45}\text{Sc} \rightarrow \pi^+\pi^+ n {}^{44}\text{Ca}$  phase space simulations, which are normalise to the  $\pi^2\pi$  data. On the theoretical side, calculations for the  $\pi^+ \rightarrow \pi^+\pi^+$  channel provide a degree of agreement with data similar to that found for the  $\pi^+ \rightarrow \pi^+\pi^-$  channel.

The study of the  $T_\pi$  observable completes the present discussion. It confirms the framework already sketched out by the study of the previous observables, i.e.  $M_{\pi\pi}$  and  $\Theta_{\pi\pi}$ . The  $\pi^+ \rightarrow \pi^+\pi^+$  reaction channel can be explained in terms of both model calculation and phase

Table 2: Experimental total cross sections of the  $\pi^+ \rightarrow \pi^+\pi^-$  ( $+-$ ) and  $\pi^+ \rightarrow \pi^+\pi^+$  ( $++$ ) reaction channels on  $^{45}\text{Sc}$  as a function of the pion incident energy  $T_{\pi^+}$ . The uncertainties associated to the *phase - space* cross sections are omitted since they do not exceed the uncertainties of the *linear* cross sections. In the last two columns the  $\sigma_T^{+-}/\sigma_T^{++}$  ratios are reported for Sc and H, respectively.

$T_{\pi^+}[\text{MeV}]$	$\sigma_T [\mu\text{b}]$				$\sigma_T^{+-}/\sigma_T^{++}$	
	<i>linear</i>		<i>phase space</i>		$^{45}\text{Sc}$	$^1\text{H}$
	$+-$	$++$	$+-$	$++$		
240	$1225 \pm 164$	$143 \pm 19$	1209	141	$8.6 \pm 1.6$	$7.1 \pm 1.2$ [25]
260	$2595 \pm 348$	$347 \pm 47$	2559	341	$7.5 \pm 1.4$	$6.1 \pm 0.9$ [25]
280	$4263 \pm 571$	$507 \pm 68$	4233	505	$8.4 \pm 1.6$	$7.4 \pm 1.0$ [25]
300	$6660 \pm 892$	$640 \pm 86$	6643	637	$10.4 \pm 2.0$	$9.6 \pm 1.5$ [25]
320	$9160 \pm 1227$	$826 \pm 110$	9148	824	$11.1 \pm 2.1$	$12.4 \pm 3.0$ [26]

space. The  $\pi^+ \rightarrow \pi^+\pi^-$  data are only partially clarified; in the present case, the model predictions fail to describe the high-energy tail of the  $T_\pi$  distributions, which follow phase space.

#### 6.4 The $\pi 2\pi$ total cross sections, $\sigma_T$

With the CHAOS spectrometer one can directly determine  $d^3\sigma/d\mathcal{O}_{\pi\pi}d\Omega_\pi d\Omega_\pi$ , where  $\mathcal{O}_{\pi\pi}$  represents a generic observable,  $d\Omega_\pi$  is the solid angle into which a charged pion is scattered and  $d\Omega_\pi = d\cos(\Theta_\pi)d\Phi_\pi$ . In order to assess  $\sigma_T$ , the multiple differential cross section has to be summed over  $\mathcal{O}_{\pi\pi}$  and  $\Omega_\pi$ 's. The limited  $\Phi$ -acceptance of CHAOS, however, allows the determination of  $d\sigma/d\Phi_{\pi\pi}$  only at  $\Phi_{\pi\pi} = 0^\circ$  and  $\Phi_{\pi\pi} = 180^\circ$ , where  $\Phi_{\pi\pi} \equiv \Phi_{\pi_1\pi_2} = |\Phi_{\pi_1} - \Phi_{\pi_2}|$ . Within this interval, the  $\Phi$ -dependence of the  $\pi 2\pi$  reaction is presently assumed either to behave linearly, or to follow the  $^{45}\text{Sc}(\pi^+, \pi^+\pi^\pm N)^{44}\text{X}$  phase space (see Sec. 3, and Fig. 4 for details). In this framework, the results obtained for  $\sigma_T$  are those reported in Table 2. In the last two columns, the ratios  $\sigma_T^{+-}/\sigma_T^{++}$  for the two reaction channels are listed. For a given  $T_{\pi^+}$ , the ratios for Sc and H agree within the error bars, which implies that a similar reaction mechanism underlies the  $\pi 2\pi$  reaction whether it occurs in the nucleon or in nuclei. This confirms that the  $\pi 2\pi$  reaction in nuclei is a quasifree process.

### 7. Existing $\pi 2\pi$ results

Two collaborations have recently presented their studies of  $\pi\pi$  dynamics in nuclear matter in proximity of the  $2m_\pi$  threshold. These are the Crystal Ball (CB) Collaboration at the AGS and the TAPS collaboration at MAMI. Comparisons can only be made with the

general features of the data, since pion pairs are produced by different reactions, or different isospin channels are studied, or different energies and nuclei are examined in the different experiments.

The CB Collaboration has presented results on the  $\pi^-A \rightarrow \pi^0\pi^0A'$  reaction for A:  $H$ ,  $^{12}C$ ,  $^{27}Al$  and  $^{64}Cu$ , at an incident pion energy of  $T_{\pi^-}=291.6$  [22]. Neutral pion pairs have  $I=0$ , therefore they can be directly compared to  $\pi^+\pi^-$  pairs [1, 7, 15, 21]. A recent article [23] compares the CB and CHAOS data, pointing out the relevant common features shared by the two data sets. The observable  $\mathcal{C}_{\pi\pi}^A$  is of particular interest in the comparison.  $\mathcal{C}_{\pi\pi}^A$  is proportional to the ratio of  $M_{\pi\pi}^A$  to  $M_{\pi\pi}^H$  [6, 7]. Consideration of such a ratio lessens the importance of the difference in the CB ( $\sim 93\%$  of  $4\pi$ ) and CHAOS ( $\sim 12\%$  of  $4\pi$ ) acceptances. Comparison shows that the behaviour of  $\mathcal{C}_{\pi^0\pi^0}^C$  and  $\mathcal{C}_{\pi^+\pi^-}^C$  is similar over the entire energy range.

$\pi\pi$  dynamics in nuclear matter has been also studied by the TAPS Collaboration. TAPS has used the photoproduction reaction  $\gamma \rightarrow \pi\pi$  on  $H$ ,  $^{12}C$  and  $^{208}Pb$ , at photon energies from 400 to 460 MeV[24]. At these energies, gammas can penetrate to the interior of nuclei, therefore probing nuclear densities ( $\rho \sim 0.35\rho_n$  for  $^{12}C$  and  $\rho \sim 0.65\rho_n$  for  $^{208}Pb$ ) higher than the pions in the present work ( $\rho \sim 0.36\rho_n$ ). In the case of TAPS, medium effects on the  $I=0$   $\pi\pi$  interacting system are understood to be broader than the CHAOS ones, but the nuclear distortions on the two pions being detected are also broader, which has an impact on the  $M_{\pi\pi}^A$  cross section. Therefore, a simple comparison of  $\mathcal{C}_{\pi^0\pi^0}^A$  to  $\mathcal{C}_{\pi^+\pi^-}^A$  may be misleading, since distortions do not affect  $M_{\pi\pi}^H$ . TAPS has redefined the composite ratio  $\mathcal{C}_{\pi\pi} \equiv M_{\pi\pi}^{Pb}/M_{\pi\pi}^C$ . With this new definition, the TAPS  $\mathcal{C}_{\pi\pi}$  agrees well with the CHAOS  $\mathcal{C}_{\pi\pi}$  (Ref. [24]). In addition, strong medium modifications have been observed only for the  $\gamma \rightarrow \pi^0\pi^0$  reaction channel; that is, for pion pairs interacting in the  $I=J=0$  channel. Medium effects on the isospin  $I=1$   $\pi\pi$  pairs have not been detected. Further points of contact between the TAPS and the CHAOS results are discussed in Ref. [24].

## 8. Conclusions

This article presents the results of an exclusive measurement of the pion-production  $\pi^+ \rightarrow \pi^+\pi^\pm$  reactions on  $^{45}Sc$ , at incident pion energies of 240, 260, 280, 300 and 320 MeV. In previous measurements the same reaction has been examined on  $^2H$ ,  $^4He$ ,  $^{12}C$ ,  $^{16}O$ ,  $^{40}Ca$  and  $^{208}Pb$  nuclei, at an incident pion energy of  $\sim 280$  MeV [1, 2, 3, 4, 5, 6, 7]. A two-fold interest has been driving these measurements: understanding the general traits of the pion-production reaction in nuclei, and studying the  $\pi\pi$  dynamics in nuclear matter. To this end, the CHAOS magnetic spectrometer at TRIUMF has been used, which permitted the analysis of  $\pi^+\pi^+$  and  $\pi^+\pi^-$  pairs simultaneously. The study of the medium modifications of the  $\pi^+\pi^-$  interacting system is of central importance, being the lightest system which carries the  $I=0$   $J=0$  quantum numbers, that is, the quantum numbers of the QCD vacuum. At the present

energies, the I=2 pion pairs interact very weakly, thus, only weak medium modifications on the  $\pi^+\pi^+$  system are expected. Therefore, the comparison of the two isospin channels yields direct indications of the nuclear medium effects on the  $(\pi\pi)_{I=J=0}$  system, that is, on the  $\sigma$  meson.

The A- and T-dependence studies of the  $\pi 2\pi$  reaction lead to the following conclusions.

1. The  $\pi 2\pi$  reaction in nuclei is a quasifree process, which involves a single nucleon  $\pi N \rightarrow \pi\pi N$ .
2. An analysis of the  $p_{\pi\pi}$ -dependence of  $M_{\pi\pi}$  reveals that near the  $2m_\pi$  threshold  $\pi\pi$  pairs carry the highest momenta available, and the opening angle distribution of  $\pi^+\pi^-$  pairs is peaked at  $\sim 0^\circ$ . This behavior is not explained by the reaction phase space or by theory.
3. The  $\pi 2\pi$  data are compared with a complete model of the pion-production reaction[15]. At the present energies, calculations indicate that the average nuclear density at which the process occurs is  $\rho \sim 0.36\rho_n$ , that is, the process is confined to the nuclear skin.
4. The observables  $M_{\pi\pi}$ ,  $\Theta_{\pi\pi}$  and  $T_\pi$  have been carefully examined and compared to model calculations and reaction phase space, both of which take the CHAOS acceptance into account. The dynamics of the  $\pi^+ \rightarrow \pi^+\pi^+$  channel is well explained by theory. Phase space provides a good description of the kinematic behaviour of the reaction over a wide range of energies. The nuclear medium does not detectably modify the  $(\pi\pi)_{I=2J=0}$  interaction. For example, the threshold behavior of  $M_{\pi^+\pi^+}$  depends negligibly on A and T. This also indicates that pion final state interactions cannot account for the enhancement observed at around the  $2m_\pi$  threshold. The dynamics of the  $\pi^+ \rightarrow \pi^+\pi^-$  channel is far more varied. For the elementary  $\pi N \rightarrow \pi\pi N$  reaction, the  $M_{\pi^+\pi^-}$  strength at around threshold is depleted over a wide range of incoming pion energies, from 223 to 305 MeV Ref. [25] and this work Fig. 9. Thus the terms forming the elementary amplitude must cancel out. In nuclear matter,  $M_{\pi^+\pi^-}$  rapidly gains strength, which is not caused by the final state interactions of pions with the residual nucleus. Therefore, either the medium removes cancellations or it produces new events. According to the authors of Refs. [9, 10], an event is the appearance of the  $\sigma$  meson, a genuine QCD system formed by a  $q\bar{q}$  state, which largely reshapes its spectral function in response to nuclear matter. The  $M_{\pi^+\pi^-}$  threshold strength is primarily due to this occurrence. However, this basic result is not corroborated by a model of the  $\pi 2\pi$  reaction. The model used in this article accounts for the pion-production process [15]. At around threshold,  $M_{\pi^+\pi^-}$  builds up strength via the P-wave coupling of pions to  $p$ - $h$  and  $\Delta$ - $h$  nuclear excitations. This process also underlays the dynamical origin of the  $\sigma$  meson: a  $\pi\pi$  interacting state in the I=J=0 channel. This resonant state is found to drop in mass and width at finite densities, i.e. at  $\rho < \rho_n$  [27]. However, the  $\sigma$

strength at around threshold is insufficient to explain the data. This specific issue deserves the attention of theorists, since it is of primary importance in the understanding of whether the invariant mass shift toward threshold is due to the partial restoration of chiral symmetry or to other essential events. Standard nuclear effects are already accounted for by the model used in the present analysis. This general conclusion also applies to the  $\Theta_{\pi\pi}$  and  $T_\pi$  observables.

5. The  $\pi 2\pi$  results obtained by the CHAOS Collaboration have been compared to the results of the CB and the TAPS Collaborations, which are the only available ones. The results discussed in the CHAOS articles share relevant common features with the results presented by these two collaborations. The discussion over the composite ratio  $\mathcal{C}_{\pi\pi} \equiv M_{\pi\pi}^A/M_{\pi\pi}^H$  has been only briefly developed since it is the subject of a forthcoming article.

## Acknowledgments

The authors would like to acknowledge the support received from TRIUMF. The present work was made possible by grants from the Istituto Nazionale di Fisica Nucleare (INFN) of Italy, the National Science and Engineering Research Council (NSERC) of Canada, the Australian Research Council and the German Ministry of Education and Research (BMBF 06TU987). The authors would also like to acknowledge useful discussions with Z. Aouissat, G. Chanfray, T. Kunihiro, E. Oset and P. Schuck. A special thank goes to M. Vicente-Vacas for the assistance received when using his code.

## References

- [1] F. Bonutti *et al.*, Phys. Rev. Lett. **77**, 603(1996).
- [2] D. Vetterli *et al.*, Nucl. Phys. **A548**, 541(1992).
- [3] F. Bonutti *et al.*, Phys. Rev. **C55**, 2998(1997).
- [4] N. Grion *et al.*, Nucl. Phys. **A492**, 509(1989).
- [5] F. Bonutti *et al.*, Nucl. Phys. **A638**, 729(1998).
- [6] F. Bonutti *et al.*, Phys. Rev. **C60**, 018201(1999).
- [7] F. Bonutti *et al.*, Nucl. Phys. **A677**, 213(2000).
- [8] E. M. Aitala *et al.*, Phys. Rev. Lett. **89**, 770(2001).
- [9] T. Hatsuda and T. Kunihiro, Phys. Lett. **B185** 304(1987); T. Hatsuda and T. Kunihiro, Phys. Rep. **247** 221(1994); T. Kunihiro, Prog. of Theor. Phys. Suppl. **120** 75(1995); S. Chiku and T. Hatsuda, Phys. Rev. **D57**, 6(1998); T. Hatsuda, T. Kunihiro and H. Shimizu, Phys. Rev. Lett. **82** 2840(1999).
- [10] Z. Aouissat G. Chanfray, P. Schuck and J. Wambach, Phys. Rev. **C61** R12202(2000); D. Davesne Y.J. Zhang and G. Chanfray, Phys. Rev. **C62** 024604(2000);
- [11] P. Schuck W. Nörenberg and G. Chanfray, Z. Phys. **A330**, 119 (1988).
- [12] G. Chanfray, Z. Aouissat, P. Schuck and W. Nörenberg, Phys. Lett. **B256**, 325 (1991).
- [13] Z. Aouissat R. Rapp, G. Chanfray, P. Schuck and J. Wambach, Nucl. Phys. **A581**, 471 (1995)
- [14] R. Rapp, J. W. Durso, Z. Aouissat G. Chanfray, O. Krehl, P. Schuck J. Speth and J. Wambach, Phys. Rev. **C59**, R1237 (1999).
- [15] M. J. Vicente-Vacas and E. Oset, Phys. Rev. **C60**, 064621(1999).
- [16] H. C. Chiang, E. Oset and M. J. Vicente-Vacas, Nucl Phys. **A644**, 77(1998);
- [17] E. Oset and M. J. Vicente-Vacas, Nucl Phys. **A678**, 424(2000).
- [18] E. Oset and M. J. Vicente-Vacas Nucl. Phys. **A446**, 584(1985).
- [19] G.R. Smith *et al.*, Nucl. Instr. and Meth. in Phys. Res. **A362**, 349 (1995).
- [20] F. Bonutti, S. Buttazzoni, P. Camerini, N. Grion and R. Rui, Nucl. Instr. and Meth. in Phys. Res. **A350**, 136 (1994);

- [21] D. Loshe, J. W. Durso, K. Olinde and J. Speth, Phys. Lett. **B234**, 235 (1990).
- [22] A. Starostin *et al.*, Phys. Rev. Lett. **85**, 5539(2000).
- [23] P. Camerini *et al.*, Phys. Rev. **C64**, 067601(2001).
- [24] V. Metag for the TAPS and A2 Collaboration, IPN Orsay Workshop on *Chiral Fluctuations in Nuclear Matter*, Sept 26-28,2001, Paris, France; and Messchendorp *et al.*, nucl-ex /0205009.
- [25] M. Kermani *et al.*, Phys. Rev. **C58**, 3419 (1998).
- [26] G. Kernel *et al.*, Phys. Lett.. **B216**, 244 (1989); G. Kernel *et al.*, Z. Phys. **C48**, 201 (1990).
- [27] M. J. Vicente-Vacas and E. Oset arXiv:nucl-th/0204055, 23 Apr 2002.